





Cite this: *Green Chem.*, 2021, **23**, 9109

One-pot production of oxygenated monomers and selectively oxidized lignin from biomass based on plasma electrolysis†

Lusi A, ^a Harish Radhakrishnan,^a Hui Hu^b and Xianglan Bai ^{*a}

Herein, we report a novel method to obtain oxygenated chemicals and high-quality lignin from biomass in one-pot using a single step process. Plasma electrolysis of red oak was conducted by applying high-voltage alternating current electricity in γ -valerolactone using sulfuric acid as the electrolyte. Red oak was completely solubilized to produce levoglucosenone and furfural as the two major monomers with the respective yields of up to 44.9 mol% and 98.0 mol%. During the conversion, an oxidized lignin was also simultaneously produced in high purity. The valorization potential of the plasma electrolysis-derived lignin evaluated using the pyrolysis method showed that depolymerization of this lignin could produce significantly higher yields of phenolic monomers than the natural lignin or the lignin isolated during conventional solvolysis. Our investigation showed that benzylic carbon of the natural lignin was selectively modified during plasma electrolysis to limit the formation of interunit C–C bonds, significantly improving the subsequent lignin valorization to aromatic monomers. Overall, this study demonstrated a simple green approach to improve chemical production without using costly catalysts or tedious biomass fractionation. This study also presented a novel and highly efficient way to modify lignin for enhanced valorization.

Received 9th September 2021,
Accepted 15th October 2021

DOI: 10.1039/d1gc03315h

rsc.li/greenchem

1. Introduction

Lignocellulosic biomass is an abundant renewable resource of clean energy and green products to supplement the increasing energy demand and mitigate the environmental degradation caused by fossil fuel dependence.¹ Polysaccharides in biomass are proven to be an excellent feedstock for chemical production. Various chemicals, including platform chemicals and specialty chemicals, could be obtained from cellulose and hemicellulose through deconstruction and catalytic upgrading.^{2,3} Lignin, on the other hand, can supply renewable aromatics.^{4,5} However, enabling market competitive bio-based chemicals is currently facing significant challenges due to their high production costs.

Bio-based chemicals are usually produced using biological and thermochemical routes.^{1,6–9} Biomass fractionation could increase the polysaccharide accessibility by solvents or enzymes and reduce the negative impacts caused by lignin and its derivatives.^{10–13} In traditional biorefinery approaches, cellulose or delignified pulp obtained from biomass pretreatments were used as the feedstock for producing chemicals and

advanced biofuel molecules. The major disadvantage is that biomass fractionations using harsh chemicals and severe reaction conditions usually result in low-quality lignin with little economic value other than being used as boiler fuels.^{14–16} Although lignin-derived monomers can be valuable platform chemicals for wide applications, depolymerizing the isolated lignin produces very low monomer yields due to lignin's recalcitrant nature for deconstruction and the formation of stable carbon–carbon bonds during the biomass pretreatments.¹⁷ The poor valorization of lignin has greatly hindered the economic feasibility of the biorefineries. In recent years, the lignin-first biorefinery concept was proposed to directly depolymerize the natural lignin during biomass pretreatments by employing solvents, metal catalysts, and hydrogen.^{18–20} Specifically, biomass was converted in pressurized alcohols or cyclic ether solvents at 180–250 °C for hours. Heterogeneous redox active catalysts and hydrogen gas were used during the processes to catalytically convert the isolated lignin to produce stable lignin bio-oil composed of monomers and oligomers. In the meanwhile, a carbohydrate pulp mixed with spent solid catalysts were also obtained. While such catalytic-reactive fractionations of biomass could improve lignin valorization, the recovery of catalyst from the carbohydrate pulp and mass transfer limitation within batch reactors can be problematic.^{21,22} To address the catalyst recovery issue, the biomass fractionations were performed using flow-through reactors to obtain catalyst-free carbohydrate pulps. However, flow-through reactors signifi-

^aDepartment of Mechanical Engineering, Iowa State University, Ames, IA 50011, USA.
E-mail: bxl9801@iastate.edu

^bDepartment of Aerospace Engineering, Iowa State University, Ames, IA 50011, USA

†Electronic supplementary information (ESI) available. See DOI: 10.1039/d1gc03315h

cantly increased solvent consumption compared to batch reactors.

Alternatively, biomass was directly decomposed by using pyrolysis or solvolysis. However, thermochemical conversion of whole biomass often results in crude bio-oil composed of complex compositions and low yields of monomers because carbohydrates and lignin are deconstructed in the same process.^{23–25} In this context, directly producing chemicals from biomass in high yield and selectivity, while simultaneously obtaining higher-quality lignin would significantly advance the current practices of biorefineries. Enabling such will simplify the conversion process, reduce production costs, improve lignin valorization, and therefore enhance economic profitability of the biorefineries. One-pot conversion of biomass for chemicals was explored in previous studies by employing heated and pressurized solvents containing catalysts. For example, Cai *et al.* converted woody biomass in tetrahydrofuran (THF) and water co-solvent to produce furfural (FF), 5-hydroxymethylfurfural (HMF), and levulinic acid (LA).²⁶ Luterbacher *et al.* converted biomass in γ -valerolactone (GVL) and water co-solvent to produce soluble sugars.²⁷ The resulting lignin was further upgraded using catalysts and hydrogen.²⁸ Bai *et al.* converted switchgrass in 1,4-dioxane to produce levoglucosan (LG), FF and recovered soluble lignin in a single step.²⁹ In their previous study, Chen *et al.* converted biomass using aqueous choline chloride/methyl isobutyl ketone biphasic solvent to produce FF and recovered cellulose pulp and soluble lignin.³⁰ Although the previous studies demonstrated the possibility of producing chemicals without pre-fractionating biomass, the isolated lignin often had moderate quality, which can hinder the subsequent upgrading of the lignin. Furthermore, energy efficiency and reaction rate could be improved for the solvent-based reactions.

Non-thermal plasma (NTP) is considered a novel low-energy technology for biomass conversion.^{31–33} Plasma is a partly ionized gas consisting of electrons, ions, free radicals, and atoms.^{33–35} It is usually generated by applying an external electric field to dielectric mediums. Inside NTP discharge, electron temperatures are much higher than the temperatures of heavier plasma species.³⁶ Due to this thermal non-equilibrium between the electrons and other plasma species, discharge temperatures of NTP are usually low near room temperature. Because NTP can create a chemically reactive environment at mild temperatures using low energy inputs, it has wide applications in industries, such as biomedical, food industries, polymer processing, and wastewater treatment, as a green and low-energy technology.^{33,37–40} Recently, NTP is also emerging as an unconventional way to promote biomass conversion and reduce energy consumption.^{31,32,41–44} As low-cost renewable electricity becomes increasingly available, employing plasma driven by renewable electricity to convert biomass is highly attractive in terms of economic and environmental sustainability. Attributed to unique plasma physical chemistry, the working principle of biomass conversion by NTP differs from conventional thermochemical technologies. Inside plasma discharge, free electrons liberated from excited molecules and

atoms collide with other atoms and molecules to generate ions and radicals independent of the system temperatures.^{35,45} When biomass is exposed to plasma discharge, the energy transfer associated with collision impact and the interaction between the plasma species and biomass can cleave organic bonds and initiate other chemical reactions. Depending on the type of plasma species and biomass, reactions that are otherwise thermodynamically difficult or impossible at low temperatures or without the use of catalyst would become possible with the NTP-based systems. In previous studies, NTP treatment was employed to delignify biomass and decrystallize cellulose at near room temperature without using any solvents and/or catalysts.^{32,46–48} NTP was also used to control reactions and improve product yields. For example, our previous study showed that NTP pretreatment of cellulose followed by pyrolysis could increase LG yield from 58.2 wt% to 78.6 wt% while decreasing the required pyrolysis temperature from 500 °C to 375 °C.⁴⁹ The higher LG yield and lowered reaction temperature were achieved due to a novel reaction mechanism of cellulose enabled by the NTP pretreatment.

It should be mentioned that gaseous plasma was employed in most of the previous studies. Very few investigated biomass conversion using plasma in liquids.^{50–56} Xi *et al.* studied plasma electrolysis of biomass in polyethylene glycol and glycerol mixture, reporting reduced energy consumption than using other technologies for converting biomass.^{54–56} However, energy saving was the sole advantage of their process as the products were low-quality bio-oils that require further upgrading. In our recent study, plasma electrolysis was employed to produce biobased chemicals for the first time. It was found that compared to the conventional cellulose conversion in polar aprotic solvents, plasma electrolysis performed in the same solvents could increase the yield of levoglucosone (LGO) and the rate for the monomer formation whereas reducing energy consumption.⁵⁷

By leveraging the knowledge gained from our previous work, a novel biomass conversion was developed in this study to produce high yields of carbohydrate-derived monomers and high-quality lignin in one pot using a single-step process. Specifically, high-voltage electricity was applied to red oak in GVL and diluted sulfuric acid to produce oxygenated monomers and a novel oxidized lignin in the absence of external reactor heating. The novel lignin was further pyrolyzed to evaluate its valorization potential for producing monomers. The advantage of plasma electrolysis was also determined by performing conventional solvolysis of biomass and comparing products.

2. Materials and methods

2.1. Materials

Northern red oak (*Quercus Rubra*) was purchased from Wood Residue Solutions (Montello, WI). The bark-free chips were first ground and then sieved to particle size ranging from 250 to 400 μm . Proximate, ultimate, and compositional analyses of

red oak are given in Table S1.† Cellulose, GVL ($\geq 99\%$ purity), FF, and 1,4:3,6-dianhydro- α -D-glucopyranose (DGP), phenol ($\geq 99\%$), guaiacol ($\geq 98\%$), syringol ($\geq 99\%$), and other aromatic compounds were purchased from Sigma Aldrich. Sulfuric acid (99.6%) was obtained from Fisher Scientific. LGO (99.9%) and LG (99.9%) were purchased from Carbosynth Ltd, and the LA was from Acros Organics. Dimethylsulfoxide (DMSO)-d6 (99.9%) and pyridine-d5 (99.9%) were purchased from Cambridge Isotopes Inc. Deionized (DI) water with an electric resistance of 18.2 M Ω was available on site.

2.2. Biomass conversion

Plasma electrolysis of biomass was performed using a 30 mL three-necked round-bottom flask containing 8 mL GVL and varied amounts of sulfuric acid. The mass of red oak was 300 mg (equivalent to 4 wt% biomass loading in the solvent), otherwise indicated. For cellulose conversion, 123 mg of cellulose (equivalent to 41 wt% of the red oak mass) was used. In cases where water was used as a co-solvent, 1 wt% of DI water was added to GVL. Two tungsten rods inserted into the solvent acted as a high-voltage electrode and a ground electrode, respectively. The high-voltage electrode was connected to an AC power supply (Suman Company, CTP-2000K) to actuate plasma.⁵⁷ Electric voltage and current were also measured using a high voltage probe (*i.e.*, P6015A from Tektronix) and a high response current probe (Pearson Electronics, Inc., Pearson 2877). The electric current–voltage waveform was monitored using an oscilloscope (Tektronix DPO3054). A stir bar was placed inside the reactor for agitation. The solvent temperature was measured by a K-type thermocouple and thermometer (Oakton TEMP 100). After conversion, the liquid product was extracted for characterization. The solid residue was collected and dried in a vacuum oven for 48 hours before weighing. The thermally-based conversion of biomass in GVL solvent was performed in an externally heated 40 mL reaction vessel under continuous agitation.

2.3. Lignin isolation

The post-reaction liquid of red oak was mixed with DI water at a 1 : 10 (v/v) ratio in an ice-cooled flask to precipitate lignin. After 48 hours, the precipitated lignin was water washed three times and vacuum dried. Milled wood lignin (MWL) was extracted from red oak using the methods described in our previous publication.¹⁷

2.4. Product characterizations

Agilent 7890B gas chromatograph (GC) equipped with mass spectrometer (MS) and flame ionization detector (FID) was used to analyze liquid products. Two ZB-1701 capillary columns (60 m \times 0.250 mm \times 0.250 μ m) were used in the GC. Initially, the GC oven temperature was held at 40 $^{\circ}$ C for 3 minutes and then heated to 280 $^{\circ}$ C at 4 $^{\circ}$ C min⁻¹. Finally, the oven was held at 280 $^{\circ}$ C for additional 4 minutes. The GC inlet temperature was maintained at 280 $^{\circ}$ C. The flow rate of helium gas was 1 mL min⁻¹, and the split ratio at the GC inlet was 20 : 1. The temperature of the FID detector was 280 $^{\circ}$ C,

and hydrogen and airflow rates were 5 mL min⁻¹. The compounds in the liquid products were identified using MS based on the NIST library. The monomer yields were quantified using FID. The instrument was calibrated by injecting five different concentrations of each compound in the GC and measuring the FID peak areas.^{58,59} All the calibration curves had regression coefficients higher than 0.99. For polysaccharide-derived monomers, carbon mole-based yields were calculated using eqn (1). FF yield was calculated per hemicellulose fraction, and LGO, DGP, LA, LG yields were calculated per cellulose fraction:

$$\text{Monomer yield (C mol\%)} = \frac{\text{Carbon mole in monomer}}{\text{Carbon mole in cellulose or hemicellulose content in red oak}} \quad (1)$$

Fourier transform infrared spectroscopy (FTIR) analysis of biomass and its derived products were carried out using a Thermo Scientific Nicolet iS10 equipped with a Smart iTR accessory. The wavenumbers ranged from 500 cm⁻¹ to 4000 cm⁻¹, and each sample was scanned 64 times at a resolution of 4 cm⁻¹ and an interval of 1 cm⁻¹.

For gel-permeation chromatographic (GPC) analysis, 25 mg of lignin was dissolved in 10 mL of THF. Dionex/Thermo Scientific Ultimate 3000 Binary Semipreparative LC System (Sunnyvale, CA) was equipped with two Agilent PLgel 3 μ m 100 \AA 300 \times 7.5 mm columns and one Mesopore 300 \times 7.5 mm column. Diode Array Detector (DAD) with THF as the mobile phase was used. The flow rate and temperature of THF were 1.0 mL min⁻¹ and 25 $^{\circ}$ C, respectively. Each sample was filtered with a 0.45 μ m filter before analysis. The GPC system was calibrated using the polystyrene standards purchased from Agilent (Agilent Technologies, Inc., Santa Clara, CA) and diluted with THF. The wavelengths used for analysis were 254 nm, 263 nm, and 280 nm. While plasma electrolysis-derived lignin (PEL) was directly analyzed, MWL lignin was acetylated before the GPC analysis to increase its solubility in THF.

For heteronuclear single quantum coherence (HSQC) nuclear magnetic resonance (NMR) measurements, 70–80 mg of lignin was dissolved in 650 μ L of 4 : 1 v/v mixture of DMSO-d6 and pyridine-d5 and sonicated for 2 hours. The spectra were collected with a Bruker Avance III 600 MHz spectrometer using the pulse sequence 'hsqcetgpsisp2.2' at 25 $^{\circ}$ C, using the following parameters: interscan relaxation delay of 0.5 s, 64 scans with the total acquisition time of 6 hours, a spectral width of 220 ppm in f1 and 12 ppm in f2, with centers around 90 ppm and 5 ppm respectively. The DMSO solvent peak was used as an internal reference (δ H/ δ C: 2.49/39.5). The data processing was carried out using MestReNova v12.0.1 software.

Fast pyrolysis of lignin was conducted in a Frontier micro-pyrolyzer system with an auto-shot sampler (Rx-3050 TR, Frontier Laboratories, Japan) and a single-stage furnace oven. During pyrolysis, a deactivated stainless-steel cup containing approximately 0.5 mg of sample was dropped into a furnace preheated to 500 $^{\circ}$ C. Helium gas was used as both sweep and

carrier gas. The vapors exiting the pyrolyzer were directly carried into a GC/MS-FID for online characterization of the products. The product identification and quantification were performed using the method described above. The phenolic monomer yields were reported per mass basis. Each pyrolysis case was triplicated, and the average values were reported.

3. Results and discussion

3.1. Plasma electrolysis of red oak

3.1.1. Rapid liquefaction of red oak. Initially, the solvent and biomass were both at room temperature. As shown in Fig. 1, the solvent temperature only slightly increased (<10 °C) when AC electricity was applied to biomass and pure GVL. GVL is a dielectric solvent due to absence of electrical charges in its molecule. When high frequency AC electricity was applied, the molecular dipole rotation within the polar molecule causes dielectric heating to slightly increase the solvent temperature. Due to its high dielectric strength of pure GVL, the dielectric breakdown did not occur even after applying the electricity voltages above 10 kV (a peak to peak voltage, same below). In comparison, adding small amounts of acid to GVL significantly reduced the voltage requirement for the dielectric breakdown. A dielectric breakdown was observed for the acid containing GVL when the electricity voltages were above 5 kV, evident by the appearance of electrical current spikes in the oscillogram for micro-discharges (Fig. S1†). Furthermore, a rapid increase of the solvent temperature was observed with the GVL with acid. As also given in Fig. 1, the solvent temperature increased from the room temperature to 163 °C within 3 minutes when an AC electricity with a voltage of 6 kV and frequency of 6 kHz was applied to the GVL containing 10.5 mM acid. Pure GVL has very high electrical resistance, barely passing electrical current. In comparison, the electrically charged cations and anions (*i.e.*, H⁺, SO₄⁻) of acid in GVL creates a passage of weak electric current between electrodes to reduce the electrical resistance of the bulk solvent, therefore

causing the Joule heating. The intensity of the Joule heating occurred to the acid added GVL was much greater than the dielectric heating in the pure GVL, increasing the solvent temperature much faster. In the acidic GVL, the locally heated solvent first generated gas bubbles near the electrodes where the electric field intensity is strongest and the Joule heating was most intense (Fig. S2†).⁶⁰ Acid addition, the increase of solvent temperature, as well the gas bubble formation all can reduce dielectric strength of a dielectric solvent, therefore lowering the voltage requirement for causing the dielectric breakdown.^{60–63} Since the dielectric breakdown was promoted, electrons and other active plasma species (*e.g.*, radicals, ions and excited atoms and molecules) could be more easily generated inside the acidic solvent by applying much lower voltages than that required in pure GVL. It was noticed that the temperature of the acidic solvent stabilized at prolonged conversion times rather than continually increasing. The stabilization temperatures did not exceed 165 °C for various test conditions although there were slight differences in the rates of the temperature increases (temperature profiles of the solvents under other test conditions are given in later sections of this article). During plasma electrolysis, the electron emission and ionization due to the dielectric breakdown and plasma formation increase the electric conductivity of the solvent to lower its electrical resistance. As a result, the intensity of the Joule heating will decrease as the plasma effect increases, stabilizing the solution temperature at a prolonged reaction time. The power consumption rapidly decreased after the dielectric breakdown and plasma formation occurred (Fig. S3†), which supports the above statement. The same phenomena was also reported in our previous publication.⁵⁷ The mass balance of red oak as a function of conversion time is shown in Fig. 2 for the case with a voltage of 7 kV and a frequency of 6 kHz applied to the solvent with 10.5 mM acid. Benefited by the combined effects of the Joule heating and the active plasma species, a rapid solubilization of red oak was observed during plasma electrolysis. Only after 10 minutes, red oak was fully solubilized. Complete solubilization of red oak was always

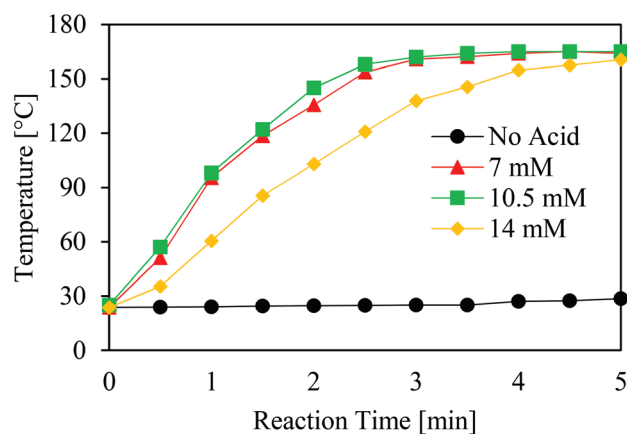


Fig. 1 The profiles of solvent temperature during plasma electrolysis with and without acid. Reaction conditions: $V = 6$ kV and $f = 6$ kHz.

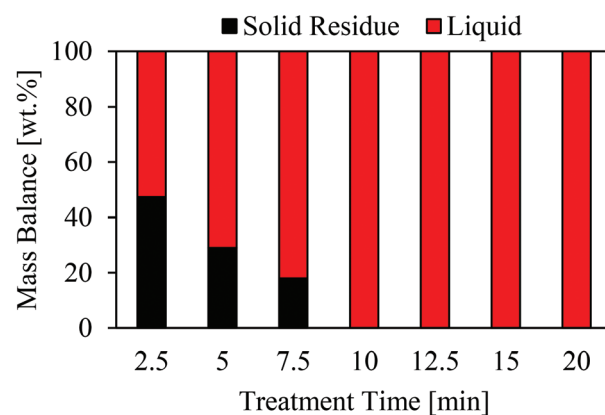


Fig. 2 Mass balance of red oak during plasma electrolysis. Reaction conditions: 10.5 mM acid, $V = 7$ kV and $f = 6$ kHz.

observed during plasma electrolysis using different experimental parameters.

3.1.2. Effect of acid. A small amount of acid added to the reaction solvent can play multiple roles during plasma electrolysis of biomass. During conventional biomass conversion in GVL, acid can strongly catalyze depolymerization and dehydration reactions even at minor concentrations.^{27,58,59,64,65} This is because the polar aprotic solvent could affect the stability of the acidic proton relative to protonated transition states, leading to accelerated reaction rates for acid-catalyzed

conversion.^{58,59} As it was described above, the acid addition also increases the solvent temperature to facilitate the formation of plasma species during plasma electrolysis. The effect of acid concentration on the monomer production was investigated by fixing the electric voltage and frequency at 6 kV and 6 kHz but varying the acid concentration. FF and LGO were two primary monomers in the liquids. Other polysaccharide-derived monomers detected by GC/MS also include LA and DGP. As shown in Fig. 3, the monomer yields and the reaction rate for producing the monomers strongly depended on acid

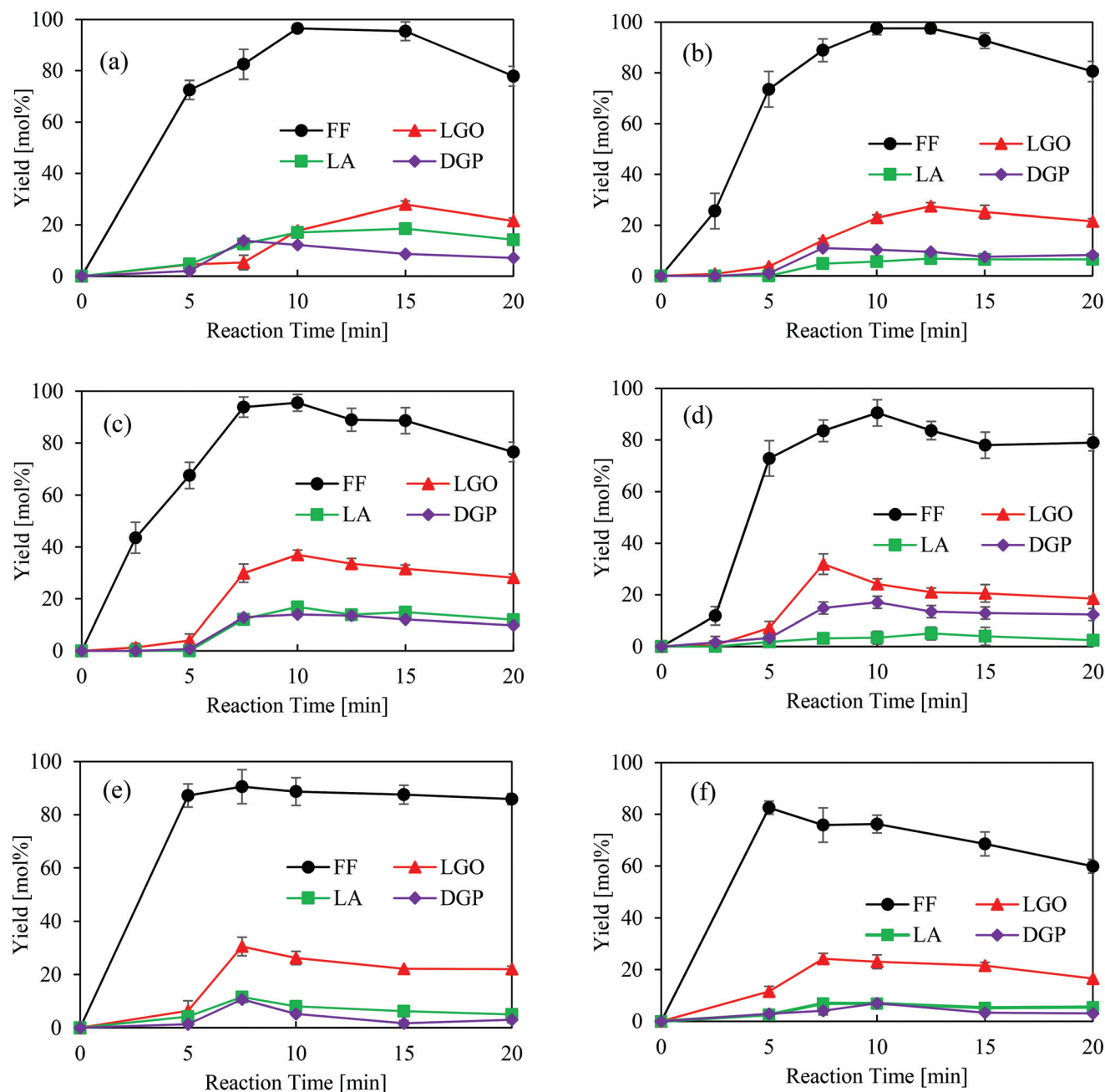


Fig. 3 Effects of acid concentration on monomer yields produced from plasma electrolysis of red oak: (a) 7 mM; (b) 9 mM; (c) 10.5 mM; (d) 12 mM; (e) 14 mM; (f) 17.5 mM. Reaction conditions: $V = 6$ kV and $f = 6$ kHz.

concentration. FF was the primary product of hemicellulose dehydration. It is an important platform chemical for solvents, polymers, and the synthesis of other chemicals.^{66,67} The maximum FF yield of 97.5 mol% was achieved using 9 mM acid, comparable to the 96.5 mol% produced using 7 mM acid. LGO was the primary product of cellulose, usually produced by dehydration reactions. It is one of the most attractive bio-based chemicals with applications in pharmaceuticals, the synthesis of bio-based solvents, and polymers.^{68,69} The optimum LGO yields ranged from 24.2 mol% to 36.9 mol% for different acid concentrations, with the highest yield obtained with 10.5 mM acid after 10 minutes. LA, a precursor molecule of pharmaceuticals, plasticizers, and additives, was also derived from cellulose.⁷⁰ LA had a maximum yield of 18.5 mol% obtained at 7 mM acid concentration. DGP was also derived from cellulose, and its optimum yield was between 6.9 mol% to 17.0 mol% for different acid concentrations. Overall, the acid with low to intermediately high concentrations were preferred for producing higher yields of FF and LGO. Despite that the rates for producing the monomers became higher with further increasing acid concentrations, the optimal monomer yields decreased. The higher acid concentrations also caused the monomers to degrade faster after their corresponding optimal yields reached. While acid in the solvent can assist plasma generation, high acid concentration can negatively impact biomass conversion because acid also catalyzes secondary reactions of biomass-derived monomers to cause degradation, repolymerization or dehydration.⁷¹ During plasma electrolysis, the electrical conductivity of the initial solvent system also depends on acid concentration in the solvent. Adding small amounts of acid can create the current passage to induce the Joule heating to contribute to the rapid increase of the solvent temperature. However, increasing acid concentrations can also cause a fall in the rate of temperature increase, which was evident when the temperature profiles of the solvents with the acid concentrations of 10.5 mM and 14 mM were compared in Fig. 1 above. The similar phenomena was also observed in our previous study for increasing acid concentration.⁵⁷ Since the number of ions proportionally increase as the acid concentration increases, the electrical resistance of the solvent decreased with increasing acid concentration. As a result, the Joule heating effect decreased when acid concentration reached an optimal.

3.1.3. Effects of voltage and frequency of electricity source.

Increasing voltage can increase both the number density and the energy-density of the plasma species. In this study, the minimum voltage required for causing the dielectric breakdown in the acidic GVL was 5 kV. Thus, the voltage effect was investigated by fixing the frequency at 6 kHz and varying the voltage between 5 kV and 8 kV. The acid concentration remained at 10.5 mM because overall highest monomer yields were obtained with this concentration. The voltage effect on the temperature profile of the solvent is shown in Fig. S4† for selected voltages. The heating rate of the solvent and the stabilization temperature were both lowest with the voltage of 5 kV. However, the differences in the rises of the solvent tempera-

tures were rather small for the voltages higher than 6 kV. As shown in Fig. 4, the highest yields of FF and LGO were only 68.8 mol% and 15.6 mol%, respectively, for the 5 kV case due to the lowest Joule heating effect and plasma effect. Increasing the voltage was found to increase the rates of LGO and FF production, improving the maximum yields of the monomers. With the voltage of 7 kV, 98.0 mol% of FF and 39.5 mol% of LGO were produced after 5 and 7.5 minutes, respectively. Similarly, high LGO and FF yields (40.8 mol% and 95.4 mol%) were also observed for the applied voltage of 7.5 kV. However, applying the even higher voltage of 8 kV had adverse effects on the monomer yields. Applying higher voltages also increased the thermal instability of the monomers in the solvent. The maximum LA yield of 16.8 mol% was produced when the voltage was 6 kV.

In comparison to the voltage effect, the effect of frequency is much more complex and less straightforward. It was previously reported that the frequency can affect the number and the lifetime of micro-discharge of the plasma, the charge intensity, the plasma current, as well as effective discharge voltage.⁷² The effect of frequency was investigated by fixing the voltage at 7 kV and varying the frequency between 5.5 kHz and 8 kHz. The temperature profiles of the solvents with varied frequencies are given in Fig. S5.† The rise of the solvent temperature became faster by increasing the frequency from 5.5 kHz to 6 kHz. However, further increasing the frequency in turn slightly lowered the heating rate. There was not much difference on the final temperature of the solvents with different frequencies. The frequency effect on the monomer yields is shown in Fig. 5. The optimum FF yield of 95.5 mol% and LGO yield of 36.9 mol% were obtained using the frequency of 6 kHz. Unlike the study on voltage effects, the reaction rates for producing monomers did not increase by applying higher frequencies. Furthermore, the optimal monomer yields and thermal stability of the monomers both decreased for applying higher frequency.

3.1.4. Effects of biomass loading and water co-solvent. The effect of biomass loading was evaluated by applying the same electric parameters to convert two different loadings of red oak (1.3 wt% and 4 wt%) in the solvent. As given in Fig. S6,† the heating rate of the solvent was slightly faster with the lower biomass loading. However, the stabilized solvent temperatures were similar with different biomass loadings. The monomer yields for the 1.3 wt% mass loading are shown in Fig. 6 for different acid concentrations. The applied voltage and frequency were the same as the conditions used in Fig. 3 for converting the higher biomass loading. The maximum LGO yield was 44.9 mol% with the lower biomass loading, obtained by using 7 mM acid. This yield is higher than the 27.8 mol% obtained with the same acid concentration, and the maximum 36.9 mol% obtained with 10.5 mM acid, both using the higher biomass loading. The maximum FF yield was 93.5 mol% by converting lower biomass loading, which was slightly lower than the maximum 97.5 mol% obtained using higher biomass loading. Optimum LA yields were comparable with the two different biomass loadings. Much lower DGP yields obtained

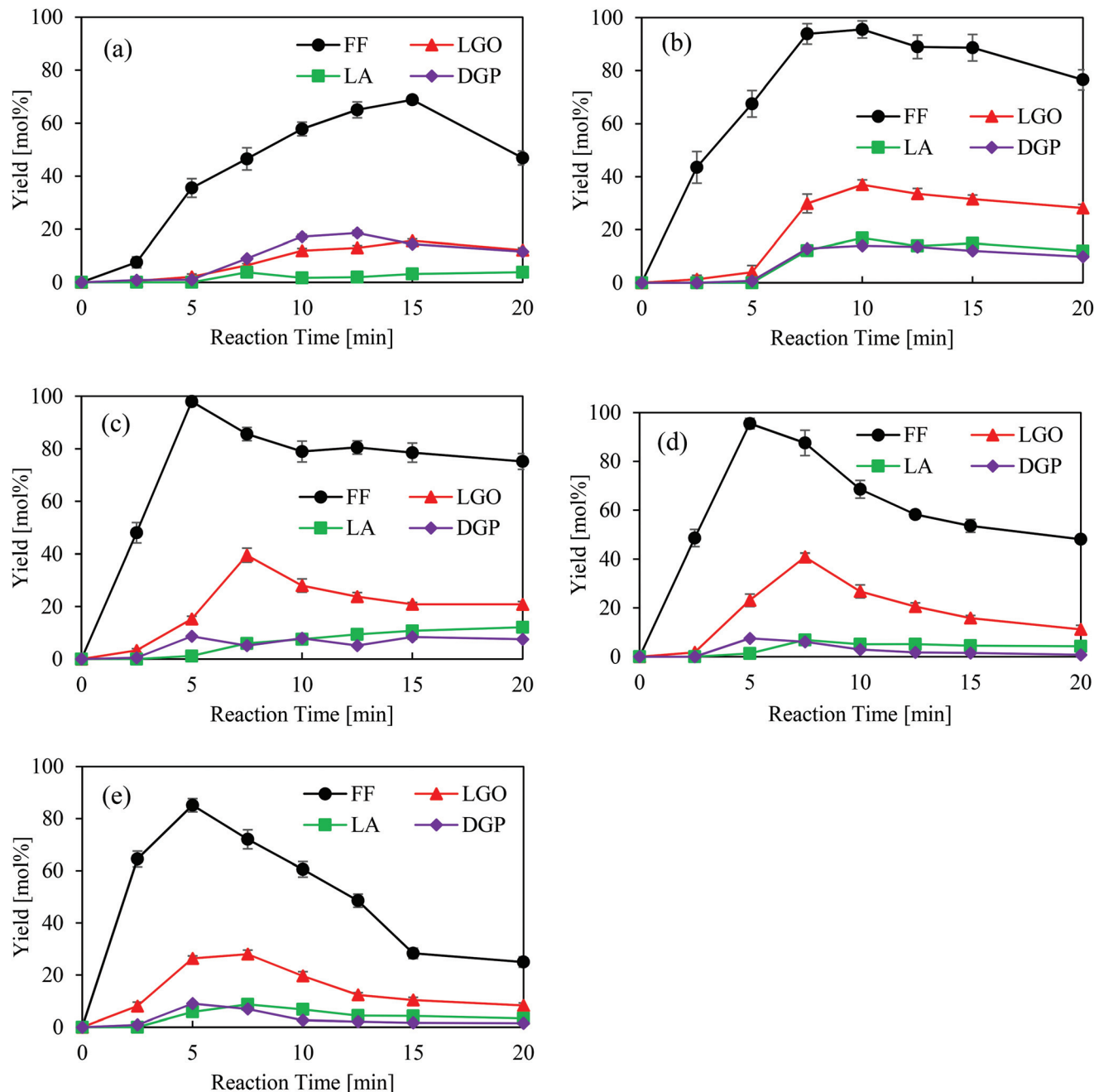


Fig. 4 The effects of electric voltage on monomer yields produced during plasma electrolysis of red oak: (a) 5 kV; (b) 6 kV; (c) 7 kV; (d) 7.5 kV; (e) 8 kV. Reaction conditions: 10.5 mM acid and $f = 6$ kHz.

using the lower biomass loading, probably because the reduced biomass loading in the solvent promotes dehydration of DGP to LGO.^{57,73}

In conventional biomass conventions in the polar aprotic solvents, the addition of water as a co-solvent affected the monomer selectivity due to acid-catalyzed hydrolysis.^{26,27,74} In this study, the effect of water addition was evaluated by adding 1 wt% of water to GVL with 10.5 mM acid. As shown in Fig. S7,[†] the water addition increased the maximum FF yield from 97.5 mol% to 98.3 mol%, whereas decreasing LGO yield

from 36.9 mol% to 31.5 mol% when the voltage of 6 kV was applied. For the applied voltage of 7 kV, the maximum yields of FF and LGO decreased from 98.0 mol% and 39.5 mol% without water to 91.5 mol% and 34.8 mol% with water. DGP and LA yields also decreased with the water addition. Water addition did not affect the solubilization of red oak. However, the rates for producing monomers decreased after adding water. The effect of water during plasma electrolysis is more than just acid-catalyzed hydrolysis. Adding water as co-solvent increased the electric conductivity of the initial solvent system,

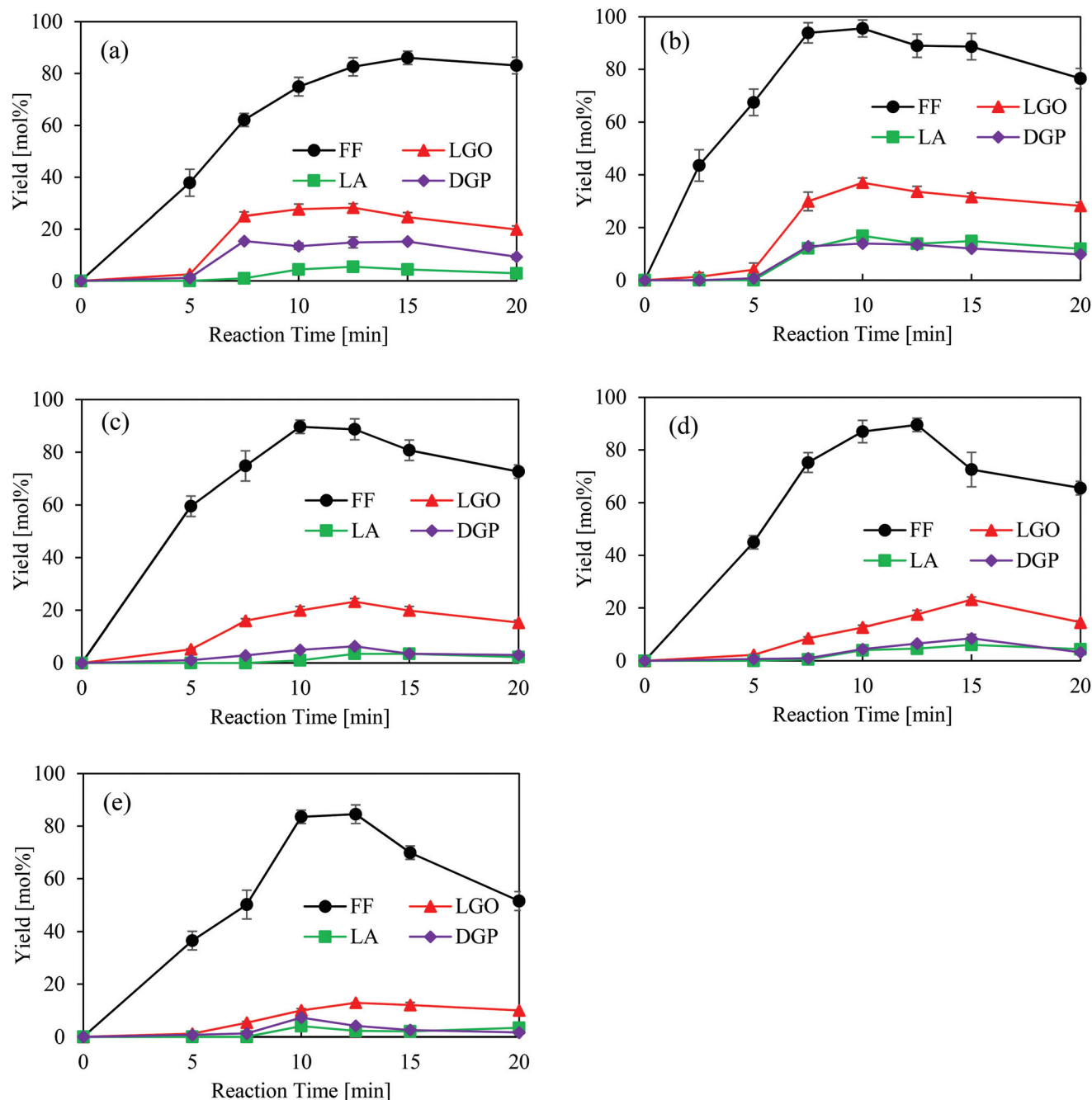


Fig. 5 The effects of electricity frequency on the monomer yields produced during plasma electrolysis of red oak: (a) 5.5 kHz; (b) 6 kHz; (c) 6.5 kHz; (d) 7 kHz; (e) 8 kHz. Reaction conditions: 10.5 mM acid and $V = 6$ kV.

evident by the decreased electric resistance of the solvent prior to the reaction from 5.04 M Ω without water to 4.26 M Ω with water. Due to the changing electric properties, the water addition can reduce the dielectric breakdown of the solvent,⁶³ influence the Joule heating, and the formation of plasma species. The temperature profile of the solvent given in Fig. S8† shows the slower solvent heating by the water addition. The heating rate became noticeably slower at the temperature above 100 °C, likely due to the heat loss caused by water evaporation from the solvent mixture. Under plasma dis-

charge, water can be dissociated to form both radicals and ions of hydrogen and hydroxyl.^{60,75} While hydrogen radicals play a key role in promoting biomass conversion during plasma electrolysis (will be discussed in later section), the hydroxyl radicals originated from water could combine with the hydrogen radicals to reduce the number of hydrogen radicals and therefore negatively affect the biomass conversion. Although the advantage of water addition was not apparent in the present study, the results suggest that plasma electrolysis of biomass can be tuned using water as a co-solvent.

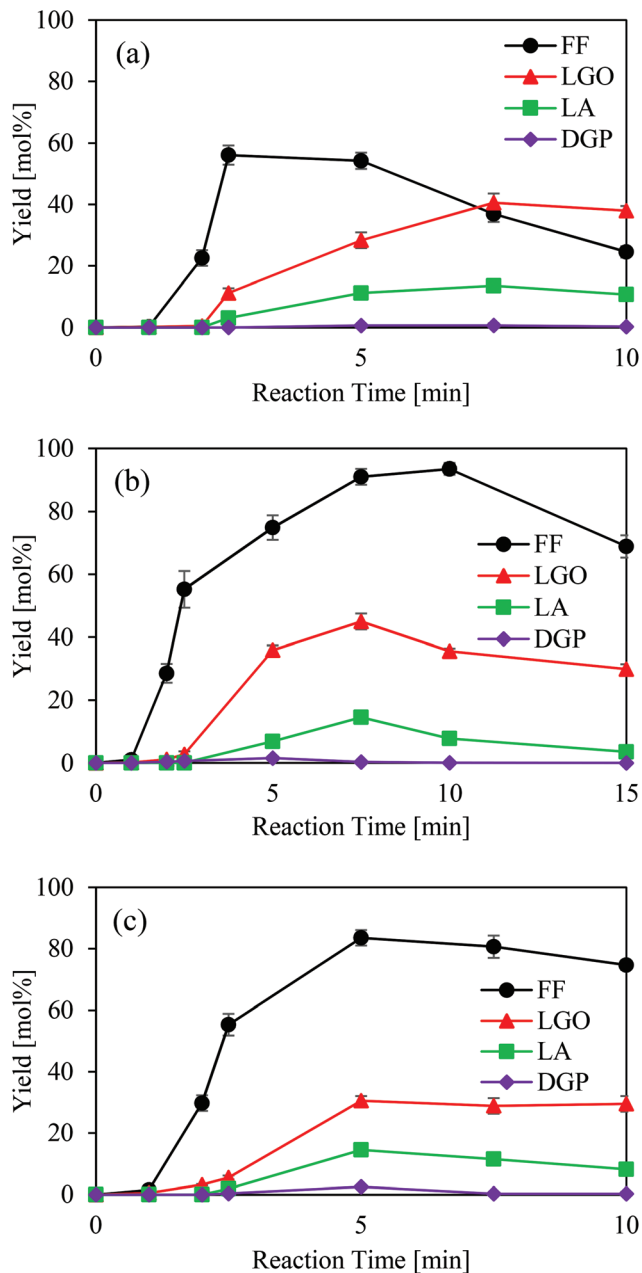


Fig. 6 Monomer production during plasma electrolysis with 1.3 wt% red oak loading and acid concentrations of (a) 3.5 mM; (b) 7 mM; (c) 10.5 mM. Other reaction conditions: $V = 6$ kV and $f = 6$ kHz.

3.2. Thermally-based conversion of red oak in GVL for comparison

As shown above, FF and LGO were selectively produced during plasma electrolysis. The effectiveness of plasma electrolysis was evaluated by converting red oak in the GVL and acid using the conventional thermally-based method. As described above, the solvent temperature could increase up to 165 °C during plasma electrolysis due to the Joule heating effect. Thus, the thermally-based conversion was conducted at 165 °C, and the mass balance results are given in Fig. 7. In the first

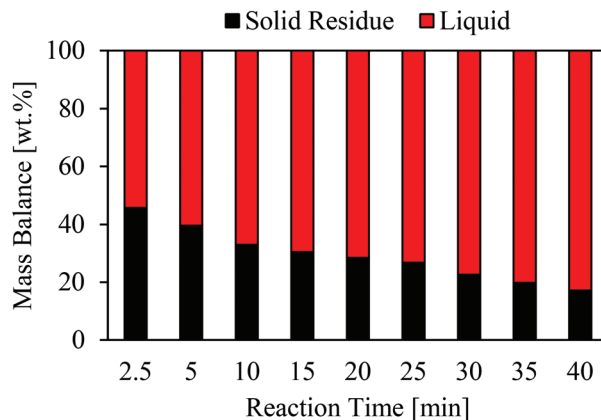


Fig. 7 Mass balance during thermally-based conversion of red oak. Reaction condition: 10.5 mM acid and 165 °C.

2.5 minutes, the liquid yield was 54.3 wt%, similar to the yield obtained during plasma electrolysis shown in Fig. 2 above. However, the conversion after that was significantly slower with the thermally-based conversion. Compared to plasma electrolysis, where red oak was dissolved entirely within 10 minutes, 17.2 wt% solid remained even after 40 minutes during the thermally-based conversion.

The monomer yields obtained using the two different conversion techniques are compared in Table 1. The maximum yields of FF, LGO, and LA from the thermally-based conversion were 84.7, 12.5, and 2.5 mol%, respectively, all produced after 35 minutes. These monomer yields are significantly lower than the corresponding monomer yields produced during plasma electrolysis using much shorter times. The rates for the monomer production were much faster for plasma electrolysis. For example, after 2.5 minutes, FF yield was only 2.5 mol% for the thermally-based conversion, whereas the yield reached 48.0 mol% during plasma electrolysis. The comparison results demonstrate that plasma electrolysis is much more effective than the thermally-based conversion for producing higher monomer yields using a significantly lower conversion time. The results also imply that although the solvent temperature increased during plasma electrolysis, the Joule heating effect alone cannot produce the presented results observed during plasma electrolysis. Noteworthy, LG was detected only during thermally-based conversion. LG was not observed during plasma electrolysis because the conventional conversion mechanism of cellulose was altered due to the plasma effect.^{49,64,74,76} The conversion mechanism of biomass during plasma electrolysis is further described in the following sections.

3.3. Understanding plasma electrolysis of biomass

3.3.1. Comparison of biomass vs. cellulose as the feed-stock. In biomass, crystalline cellulose is protected by amorphous hemicellulose and lignin *via* intermolecular bonding. Thus, directly converting whole biomass could limit the accessibility of cellulose by the solvent and acid. The derivatives of

Table 1 Monomer yields produced during conventional thermally-based conversion and plasma electrolysis of red oak

	Reaction condition	Reaction time [min]	Yield [mol%]				
			FF	LGO	LA	DGP	LG
Conventional conversion	165 °C, 10.5 mM acid	2.5	2.5	0.5	0.1	0.7	0.0
	165 °C, 10.5 mM acid	10.0	65.1	4.0	1.3	5.0	2.2
	165 °C, 10.5 mM acid	35.0	84.7	12.5	2.5	0.0	0.0
Plasma electrolysis	7 kV, 6 kHz, 10.5 mM acid	2.5	48.0	3.3	0.0	0.5	0.0
	7 kV, 6 kHz, 10.5 mM acid	5.0	98.0	15.3	1.2	8.7	0.0
	7 kV, 6 kHz, 10.5 mM acid	7.5	85.6	39.5	6.0	5.1	0.0

other biomass compositions may also interfere with cellulose conversion. In this work, plasma electrolysis of cellulose was also performed in GVL using the same acid concentration and electricity parameters to determine the effectiveness of directly converting whole biomass. For a fair comparison, the amount of cellulose mass used for the conversion was equal to the cellulose fraction in the amount of red oak converted (*i.e.*, 41 wt% of red oak). As shown in Table 2, the initial rate of LGO formation was faster by using cellulose as the starting material. Within 5 minutes, LGO yield reached 32.3 mol% for cellulose as the feedstock, compared to 15.3 mol% produced by directly converting red oak. However, the maximum LGO yield from cellulose was 40.6 mol%, similar to the 39.5 mol% using red oak both produced after 7.5 minutes. Therefore, directly converting whole biomass was as effective as converting isolated cellulose. Using red oak as the feedstock also produced overall higher LA yields in comparison to converting cellulose feedstock. The yield of FF from cellulose conversion was only between 3.2–5.2 mol%. Since lignin does not produce FF, the result supports the claim that the FF produced during plasma electrolysis of red oak was mainly derived from hemicellulose.

3.3.2. Time-resolved analysis of biomass conversion. As described above, red oak completely solubilized during plasma electrolysis. Before the complete solubilization was attained, the solids remaining in the solvent after different reaction times (2.5, 5, and 7.5 minutes) were recovered to understand how different biomass compositions convert during plasma electrolysis. The recovered solids were first pyrolyzed to gain information about the solid compositions based on their

pyrolysis products. From the GC/MS spectra shown in Fig. S9,† the major monomers in the pyrolysis products were FF, LGO, DGP, and LG for all the solids. Lignin-derived phenolic compounds were not found among the pyrolysis products of any of the solids. Evidently, the lignin fraction was quickly dissolved in the early stage of plasma electrolysis, and therefore the remaining solids were polysaccharides or their derivatives. A minor amount of mannose was detected only from the pyrolysis products of the solid recovered after 2.5 minutes. Also, while FF was mainly produced from hemicellulose, its yields from red oak during plasma electrolysis were 48.0 mol% and 98.0 mol% after 2.5 and 5 minutes, as shown in above Table 1. Therefore, it can be concluded that the conversion of hemicellulose fraction was completed within 5 minutes. Cellulose fraction took the longest time to convert because of its more stable microcrystalline structure. It is also noted from Fig. S9† that compared to pyrolysis of pure cellulose, pyrolysis of the solid residues produced LGO and DGP in much higher selectivity at the expense of decreased selectivity to LG. LGO and DGP are produced from dehydration reactions of cellulose, whereas LG is formed upon depolymerizing glycosidic chain within cellulose. Thus, this observation suggested that the solids recovered during plasma electrolysis are modified cellulose. The modified cellulose structure promoted the formation of the dehydration monomers over the depolymerization monomer when it continues to decompose.

The FTIR spectra of red oak, cellulose and the plasma electrolysis-based solids are compared in Fig. 8. There were no significant differences in the spectra of the solids recovered at different reaction times during plasma electrolysis. Compared to red oak, it is noted that the band at 1510 cm⁻¹ corresponding to the aromatic structure reduced with all the solids, while the 3200–3550 cm⁻¹ band for hydroxyl and 2840–3000 cm⁻¹ band for the C–H group became sharper. The band region below 1100 cm⁻¹, typical for polysaccharides, was nearly identical in the solids and cellulose. Thus, the observation supports the pyrolysis result described above that lignin was removed at the very beginning of plasma electrolysis. On the other hand, the 1730 cm⁻¹ band associated with C=O bonds was present in all the solids, whereas this band does not exist in cellulose. Since other features of cellulose largely remained, the cellulose chain was likely oxidized during plasma electrolysis by forming carbonyls. The band intensity of 1010 cm⁻¹ corresponding to glycosidic C–O linkage

Table 2 Monomer yield in liquid product during plasma electrolysis with red oak or cellulose as the feedstock. Reaction conditions: 10.5 mM acid, $V = 7$ kV, $f = 6$ kHz, 300 mg red oak, and 123 mg cellulose

	Reaction time [min]	Yield [mol%]			
		FF	LGO	LA	DGP
Red Oak	5.0	98.0	15.3	1.2	8.7
	7.5	85.6	39.5	6.0	5.1
	10.0	79.0	28.0	7.6	7.9
Cellulose	5.0	3.2	32.3	2.9	13.7
	7.5	4.5	40.6	4.7	10.3
	10.0	5.2	33.5	4.3	7.0

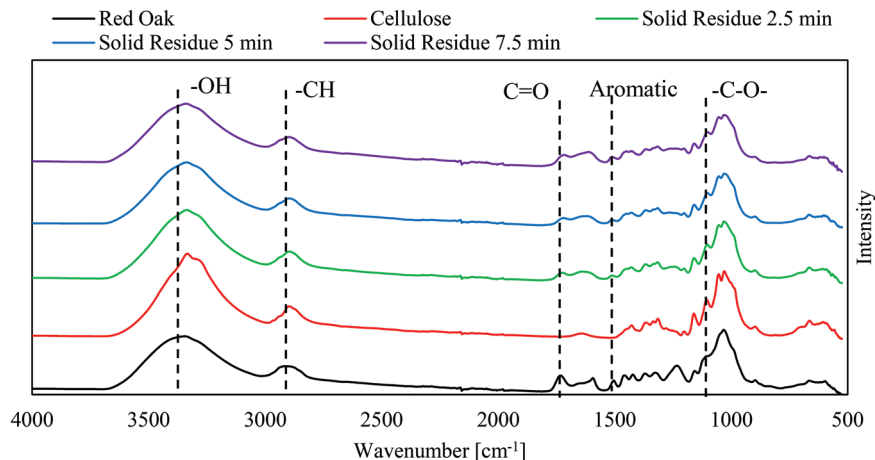


Fig. 8 FTIR spectra of red oak, cellulose, and plasma electrolysis-based solid residues recovered at the specified reaction time. Reaction conditions for plasma electrolysis of red oak: 10.5 mM acid, $V = 7$ kV and $f = 6$ kHz.

decreased in the solids recovered at longer reaction times, suggesting the glycosidic bond content in the oxidized cellulose decreased as plasma electrolysis proceeded.

The enhanced LGO formation during plasma electrolysis is associated with the oxidation of the cellulose chain, enabled by a novel radical-based mechanism.⁵⁷ During conventional acid-catalyzed cellulose conversion, cellulose is first depolymerized to LG *via* the glycosidic chain cleavage and C₁–C₆ bridging. LG is then further dehydrated to form LGO *via* DGP as the precursor.⁶⁴ During plasma electrolysis, hydrogen abstraction from cellulose occurs due to a strong electric field and electron impact. As we previously reported, the hydrogen abstraction from the glycosidic-ring carbon will lead to forming a hydroxyalkyl radical (C[•]–OH) in cellulose.^{49,57} Subsequent dehydration reaction between the hydrogen of the radical and the neighboring hydroxyl group will convert the hydroxyalkyl radical into a non-radical carbonyl (C=O). In this way, the glycosidic rings of cellulose become oxidized. LGO could form directly from the oxidized cellulose upon cleaving the glycosidic bond and bridging C₁ and C₆ of the glucose unit.⁵⁷ Meanwhile, hydrogen abstraction and dehydration on the cellulose chain during plasma electrolysis also produce DGP. DGP is further dehydrated to LGO.^{57,73} Since LGO can be produced *via* the two pathways during plasma electrolysis, the LGO yield and the rate for forming LGO are both higher in comparison to the thermally-based conversion. Since the hydrogen abstraction-assisted oxidation of cellulose predominantly occurred during plasma electrolysis, LG was not produced from the oxidized cellulose chain. This radical-based mechanism of cellulose during plasma electrolysis in polar aprotic solvents was also supported by experimental evidence provided in our previous work.⁵⁷ In the previous study, the evolution of hydrogen radicals on the solvent surface and the formation of unknown radical intermediates inside the post-reaction liquids were observed when cellulose was converted by plasma electrolysis. In the study, eliminating the *in situ* formed radicals by externally adding radical-trapping agents to

the solvent nearly terminated cellulose conversion by plasma electrolysis. However, adding the same agents had no effect on thermally-based conversion of cellulose in the same solvent. Therefore, it was confirmed that the radical intermediates are critical in promoting cellulose conversion by plasma electrolysis. The previous study further suggested that other than hydrogen abstraction from biomass, the hydrogen radicals could also be generated from the hydrogen ions of acid when the ions accept the plasma-generated electrons. The ion to radical transformation was supported by the increased pH value of the solvent during plasma electrolysis. It is likely that the radical-based dehydration by plasma electrolysis also promoted FF formation from hemicellulose.

3.4. Plasma electrolysis-derived lignin (PEL)

As described above, the lignin fraction was dissolved at the very beginning stage of plasma electrolysis. PELs and MWL extracted from red oak were analyzed to compare the valorization potential of PEL and understand how plasma electrolysis affected lignin structure. MWL was used for the comparison since it is considered to resemble natural lignin due to its gentle extraction from biomass.^{17,77,78}

3.4.1. GPC molecular weight analysis. The molecular distributions of PELs are compared to MWL in Table S2.† There were no significant differences among the molecular weight distribution of the PELs produced using different reaction times, voltages, and acid concentrations (Fig. S10†). The average molecular weights of PELs were lower than MWL, indicating lignin fragmentation occurred during plasma electrolysis. The small polydispersity values suggest that PELs have relatively uniform molecular sizes.

3.4.2. Lignin pyrolysis. Pyrolysis of lignin can be the simplest way to evaluate the valorization potential of lignin for producing aromatic chemicals. The polymeric lignin structure is depolymerized during pyrolysis to produce small molecules, including phenolic monomers and oligomers. Usually, higher monomer yields from lignin pyrolysis indicate a higher valori-

Table 3 Phenolic monomer yield produced from pyrolysis of MWL, PELs, and the thermally-based lignin. Reaction conditions for PELs: 10.5 mM acid, $V = 7$ kV and $f = 6$ kHz; Reaction condition for the thermally-based lignin: 10.5 mM acid, 165 °C, and 30 min

	MWL	PEL 10 min	PEL 15 min	PEL 20 min	Thermally- based lignin
Monomer yield [wt%]	8.61	16.92	20.86	20.91	6.96
Relative ratios of monomers					
H	1	1	1	1	1
G	10.82	5.99	4.50	4.15	9.27
S	8.96	3.42	2.49	1.88	5.67

zation potential of the lignin. The information about lignin structure can also be obtained by analyzing the pyrolysis products. The yields of total monomers produced from different types of lignin are given in Table 3. No carbohydrate-derived monomers were found among the pyrolysis products, suggesting PELs have high purity. The detailed list of the monomer species and their yields can be found in Table S3.† The typical monomers produced from both MWL and PELs include phenol, guaiacol, ethyl phenol, ethyl guaiacol, vinyl phenol, 4-vinyl guaiacol, syringol, and a few others. Additionally, pyrolysis of PELs also produced several new monomers containing phenolic carbonyl ($C_{\alpha}=O$) or propenyl-phenolic structures ($C_{\alpha}=C_{\beta}$) shown in Fig. S11.† The total yield of the phenolic monomers was 8.61 wt% with MWL. Low monomer yields from lignin pyrolysis are attributed to the complex cross-linked structure of lignin and the strong tendency of its depolymerized products to repolymerize.^{79,80} Also, hardwood-based lignin usually produces lower monomer yields than softwood or herbaceous biomass-derived lignin since high methoxyl content in hardwood lignin promotes recondensation, charring, and oligomer formation.^{17,79,81–83} The monomer yields produced from PELs were much higher, increasing from 16.92 wt% up to 20.91 wt% for the lignin recovered after longer reaction times. The fact that PELs outperformed MWL to produce significantly higher phenolic monomers is intriguing since the processes for isolating lignin from biomass usually negatively impact the valorization of natural lignin. This is because lignin fragmentation and subsequent condensation of lignin fragments during these extractions reduce the content of thermally labile β -O-4 linkages in the isolated lignin while increasing thermally stable interunit C–C bonds.^{80,81,84} Therefore, most of the previous research has focused on improving biomass fractionation techniques to extract less modified lignin.^{18,19} To determine whether the plasma electrolysis technique or the solvent system is essential in forming the high-quality lignin produced in this study, the lignin was also extracted from the thermally-based conversion of red oak in the acidic GVL and pyrolyzed. The result is included in Table 3. The total monomer yield obtained from the thermally produced lignin was only 6.96 wt%, even lower than the yield produced using MWL. Evidently, converting biomass *via* plasma electrolysis is the key for obtaining the desired high-quality lignin. The phenolic monomers produced

from different lignin shown in Table S3† were grouped into phenol (H), guaiacol (G), and syringol (S) type monomers and their relative yield ratios are also given in Table 3. The yield ratio of H : G : S monomers was 1 : 10.82 : 8.96 for MWL and 1 : 9.27 : 5.67 for the lignin recovered from the thermally-based conversion. The relative contents of S and G type monomers were high due to the abundance of S and G units in hardwood-based lignin. In comparison, the ratio was 1 : 5.99 : 3.42 for the PEL recovered after 10 minutes and 1 : 4.15 : 1.88 for the PEL collected after 20 minutes. The lower selectivity to S and G type monomers from PEL pyrolysis compared to other types of lignin implies that the natural lignin in red oak was demethoxylated during plasma electrolysis.

To further understand the modification of lignin structure during plasma electrolysis, the FTIR spectra of PELs and MWL are compared in Fig. 9. The band at 1510 cm^{-1} is for aromatic skeleton vibration. Since the aromatic ring is thermally stable, its band intensity can be used as a reference to evaluate the changes in other functional groups of lignin. Compared to MWL, the band region of $3200\text{--}3550\text{ cm}^{-1}$ stands for (aliphatic- and phenolic-) hydroxyls decreased in PELs. The band at 1325 cm^{-1} for S and G structures also decreased, probably caused by demethoxylation of the lignin. In addition, the band at 1030 cm^{-1} representing C–O–C ether bonds in β -O-4 and α -O-4 bonds, and the band at 1125 cm^{-1} for secondary alcohol decreased in PELs. On the other hand, the band at 1710 cm^{-1} for carbonyl groups significantly increased, and the band at 1670 cm^{-1} representing the side-chain C=C newly appeared with PELs.

3.3.3. HSQC NMR analysis. The main ^{13}C - ^1H cross-signals of PELs and MWL are shown in Fig. 10. For MWL, the structures of β -aryl ether (β -O-4), phenylcoumaran (β -5), tetrahydrofuran (β - β), methoxyl, cinnamaldehyde end-group structure (X2), and benzaldehyde end group (X3) were observed in its aliphatic chain region ($\delta\text{C}/\delta\text{H} = 50\text{--}90/3.0\text{--}5.5$ ppm). The signals originated from C_{α} , C_{β} , and C_{γ} positions at β -O-4 structure were abundantly observed since the aryl ether structure of the natural lignin was preserved in MWL. The signal of the Hibberts's ketone structure was feeble due to its low content. From the aromatic ring region ($\delta\text{C}/\delta\text{H} = 90\text{--}155/6.0\text{--}8.0$ ppm), syringyl (S), guaiacyl (G), and oxidized guaiacyl and syringol α -ketone structures (G' and S') were detected. In PELs, the signals originated from C_{α} in β -O-4 or β -5 structures disappeared entirely. The signals from C_{β} in these structures also decreased significantly. In comparison, C_{γ} signals were much less affected. Contradictory to the decreased β -O-4 and β -5 structures, HK, X3, and X2 structures increased for PELs. S and G structures were reduced in the aromatic region, whereas oxidized G' and S' structures were enhanced. Additionally, ferulate (FA) and *p*-coumarate (*p*CA) structures were newly detected for PELs. The quantified NMR results of PELs and MWL are given in Table 4. Since the signals of C_{α} and C_{β} positions in the corresponding structures were not detected, β -O-4 and β -5 contents were 0 for PELs. As expected, the S/G ratio was lower for PELs due to the demethoxylation. On the other hand, S'/S and G'/G ratios were higher for PELs, suggesting acetophenone

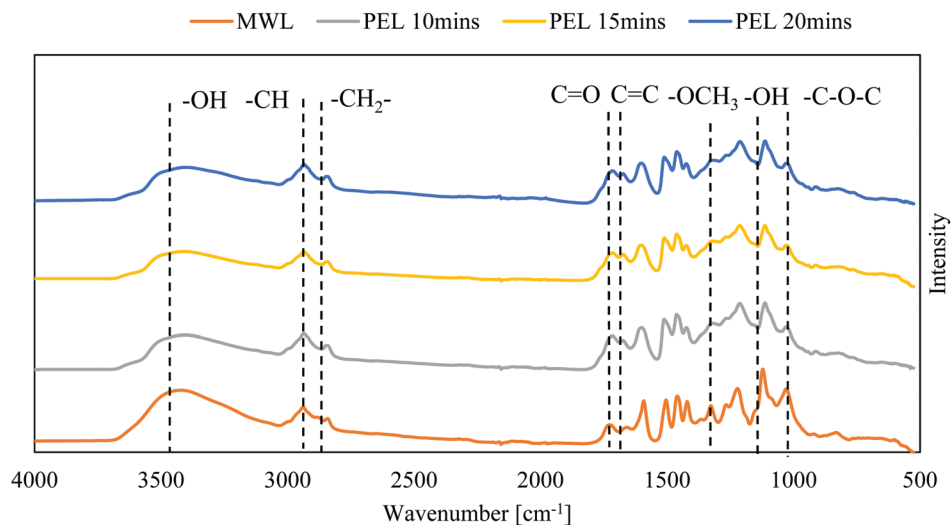


Fig. 9 FTIR spectra of MWL and PELs recovered at the specified reaction times. Plasma electrolysis reaction condition: 10.5 mM acid, $V = 7$ kV and $f = 6$ kHz.

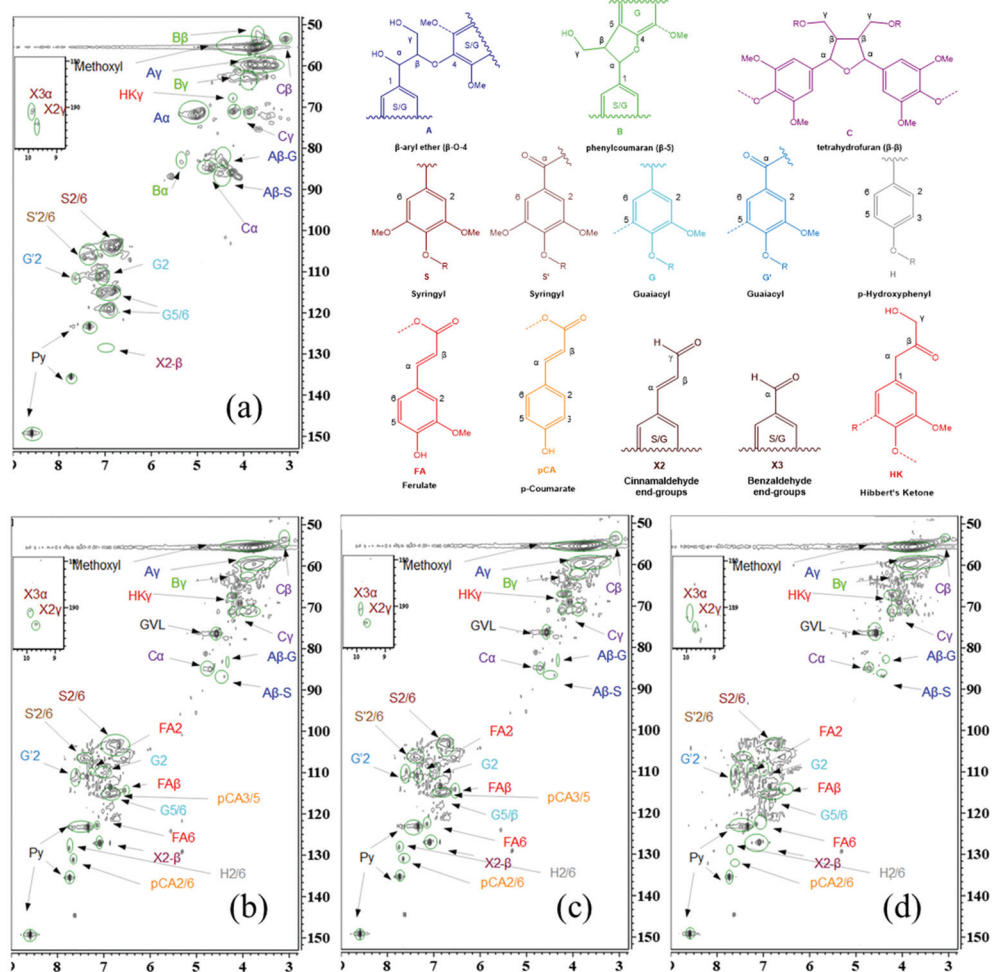


Fig. 10 HSQC 2D NMR of MWL and PELs. (a) MWL; (b) PEL 10 min; (c) PEL 15 min; (d) PEL 20 min. Plasma-electrolysis reaction condition: 10.5 mM acid, $V = 7$ kV and $f = 6$ kHz.

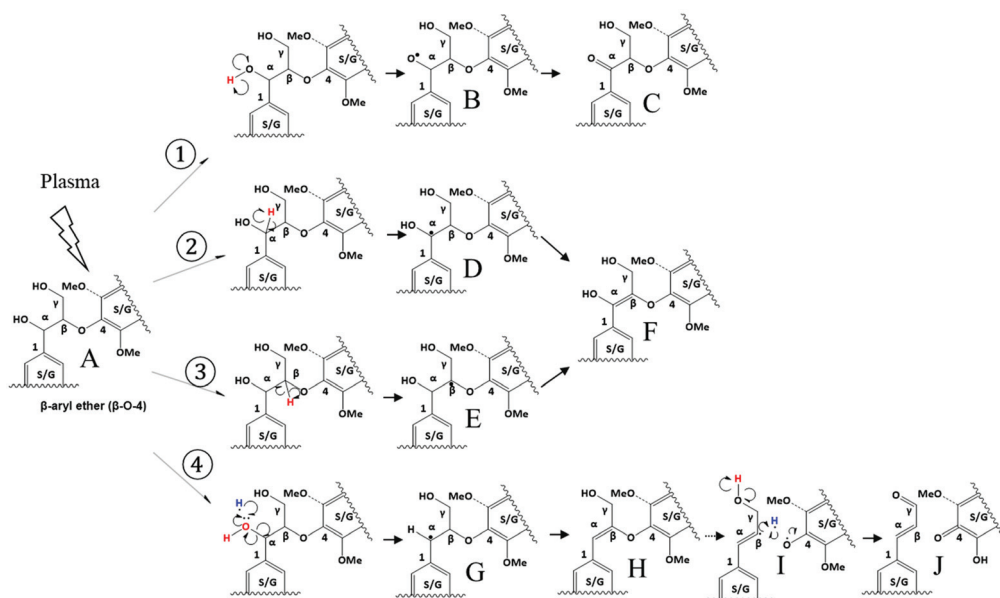
Table 4 Quantified 2D HSQC NMR results of MWL and PELs. Plasma electrolysis conditions: 10.5 mM acid, $V = 7$ kV and $f = 6$ kHz

	MWL	PEL 10 min	PEL 15 min	PEL 20 min
β -O-4 [%]	61.90	0.00	0.00	0.00
β - β [%]	14.43	12.71	10.62	10.32
β -5 [%]	2.66	0.00	0.00	0.00
X2 β [%]	0.48	16.93	25.17	34.03
FA β [%]	0.00	2.73	4.82	8.16
HK γ [%]	1.63	13.01	20.86	39.09
S/G	1.78	1.66	1.55	1.09
S'/S	0.14	0.24	0.35	0.41
G'/G	0.09	0.64	0.75	0.85

structure was promoted in PELs. It also showed that increasing reaction time during plasma electrolysis led to the PELs with higher S'/S and G'/G ratios and increased contents of HK, X2, and FA structures. What S', G', HK, X2, and FA structures have in common is that they all have a carbonyl group at their benzylic carbons (*i.e.*, $C_{\alpha}=\text{O}$). On the other hand, X2, FA, and pCA structures all have unsaturated benzylic carbon ($C_{\alpha}=C_{\beta}$) in their structures. It appears that the natural lignin was modified during plasma electrolysis to form $C_{\alpha}=C_{\beta}$ and $C_{\alpha}=\text{O}$ bonds abundantly.

The mechanism of lignin modification during plasma electrolysis is proposed in Fig. 11 using the β -O-4 structure (A) as the representative because it is the most abundant structure in lignin. The formation of new C=O and C=C in PELs could be explained using hydrogen abstraction and hydrogen radical-assisted dehydration during plasma electrolysis. Due to the plasma effect, the hydrogen atom was abstracted from the secondary alcohol at the benzylic carbon to form a $-C_{\alpha}-\text{O}^{\bullet}$ radical (B). Since this radical is highly unstable, it can easily be con-

verted to the stable non-radical isomer, $C_{\alpha}=\text{O}$ (C). The new $C_{\alpha}=C_{\beta}$ bond in PELs could be formed *via* two possible pathways. In the first pathway, the hydrogen atom is abstracted from either C_{α} (D) or C_{β} (E) positions to form a $C_{\alpha}=C_{\beta}$ bond without affecting the OH at C_{α} (F). In the second pathway, the OH at C_{α} is dehydrated by reacting with a free hydrogen radical, and the resulting $C_{\alpha}^{\bullet}-C_{\beta}$ radical (G) is subsequently converted to the non-radical $C_{\alpha}=C_{\beta}$ (H). Forming $C_{\alpha}=C_{\beta}$ and $C_{\alpha}=\text{O}$ does not cleave β -O-4 linkage. However, considering the molecular weights of PELs decreased compared to MWL, β -O-4 cleavage can also occur during plasma electrolysis due to its low dissociation energy.⁸⁵ As shown in the molecular structure I of the figure, the C_{β}^{\bullet} radical formed from the ether bond cleavage could be stabilized by the free hydrogen radicals generated during plasma electrolysis. Hydrogen radicals can be originated from biomass due to the hydrogen abstractions or from the acid when its hydrogen ions accept electrons caused by the plasma effect. The evolution of hydrogen radicals was experimentally observed in our previous study when plasma occurred in GVL with acid.⁵⁷ Therefore, the $C_{\alpha}=C_{\beta}$ formation and the cleavage of β -O-4 ether bond are both responsible for the disappeared signal of C_{β} in the β -O-4 structure of PELs. During plasma electrolysis, the primary alcohol attached to C_{γ} position can also be oxidized due to the hydrogen abstraction (J). For example, the increased X2 structure in PELs could be a result of the transformation of $C_{\gamma}-\text{OH}$ to $C_{\gamma}=\text{O}$, $C_{\alpha}-\text{OH}$ to $C_{\alpha}=C_{\beta}$, and the cleavage of β -O-4 ether bond in the natural lignin. The increased Hibbert's ketone structure in PELs is also related to the oxidation at C_{β} . In comparison, C_{γ} position of the natural lignin was much less affected than C_{α} and C_{β} positions based on their NMR signals. Therefore, the oxidation mainly occurred at the benzylic carbon. The NMR results shown in this section also well correspond to other analysis

**Fig. 11** Proposed mechanism of lignin modification during plasma electrolysis. Blue H indicates free hydrogen radicals.

results of PELs described above. The formation of new $C_{\alpha}=C_{\beta}$, $C_{\alpha}=O$, and $C_{\beta}=O$ supports the increased C=C and C=O bands observed in the FTIR spectra of PELs. The elimination of the alcohols by oxidation and/or dehydration explains the decreased OH band and secondary alcohol band in the FTIR spectra. Also, the new monomers containing $C_{\alpha}=O$ or $C_{\alpha}=C_{\beta}$ were produced exclusively from pyrolysis of PELs.

The major challenge in producing high-quality lignin with high volatility is to prevent interunit C–C coupling during lignin extraction.^{80,84} During conventional lignin extractions in an acidic environment, the dehydration of the secondary alcohol at C_{α} leads to the formation of highly reactive benzylic carbocations.^{18,80,84} Additionally, the *ortho* or *para* positions of the lignin aromatic ring are known for their high reactivity for electrophilic aromatic substitution due to rich in electrons. Thus, the subsequent reaction between the benzylic cations and the aromatic unit leads to interunit C–C bonding, rendering high thermal stability of lignin and the difficulty in deconstruction. In their previous study, Shuai *et al.* pretreated biomass with formaldehyde to block the site for the benzylic carbocation formation and avoided interunit C–C coupling.⁸⁴ The modified lignin and carbohydrate pulp obtained in their process had to be further upgraded separately. Another previous approach to prevent the C–C formation was to catalytically hydrogenolyze biomass to depolymerize natural lignin within biomass directly.⁸⁶ Although high monomer yields could be achieved using this lignin-first biorefinery approach, the carbohydrate pulp and heterogeneous catalyst must be separated before the pulp is utilized.¹⁸ Alternatively, conventionally isolated lignin was oxidized at the benzylic carbon to prevent the C–C cross-linking during lignin depolymerization.^{87–89} However, due to the non-selective nature of oxidation, selective oxidation of lignin was often challenging to achieve without producing other unstable products.^{80,84,90} Moreover, since the feedstock lignin was condensed lignin, it was challenging to obtain high monomer yield even after using harsh chemicals and catalysts for oxidation.^{80,91,92} In the present study, plasma electrolysis of red oak in the green, biomass-derivable solvent⁹³ produced a novel lignin with selectively modified benzylic carbons while converting the polysaccharide fractions into attractive monomers. In PELs, the benzylic carbon was either oxidized to $C_{\alpha}=O$ or converted to $C_{\alpha}=C_{\beta}$. Since the benzylic carbon was stabilized in such a structure, the interunit C–C coupling could be greatly mitigated. As described above, the plasma-induced hydrogen abstraction and hydrogen donation were critical in stabilizing the benzylic carbon and the C_{β} carbon. The improved volatility of PELs was also contributed by demethoxylation of lignin during plasma electrolysis because high methoxy content in lignin is known to increase coking and oligomer formation.^{79,81–83} It should be noted that PELs were pyrolyzed in this study, only to preliminary evaluate its valorization potential. As demonstrated in previous studies, using catalytic approaches will further improve the monomer yield obtainable from PELs.^{87,94,95}

4. Conclusions

Plasma electrolysis of red oak in GVL produced oxygenated monomers and an oxidized lignin in one pot using a single-step process. Benefited by the Joule heating effect and active plasma species generated during plasma electrolysis, rapid and complete solubilization of biomass could be achieved. LGO and FF were the primary monomers derived from polysaccharides, and their maximum yields were 44.9 mol% for LGO and 98.0 mol% for FF. High-purity lignin was also recovered from the solvent. Pyrolyzing PELs produced significantly higher monomer yield than the natural lignin or the conventionally extracted lignin, suggesting the presented one-pot conversion of biomass also produces high-quality lignin for depolymerization. It showed that the benzylic carbon of the natural lignin was either oxidized or dehydrated during plasma electrolysis, prohibiting the formation of interunit C–C linkage at this site. Since undesired condensation and cross-linking were greatly suppressed in the new lignin structure, the subsequent depolymerization of PELs could produce high yields of phenolic monomers. Overall, the current study showed a novel single-step approach to produce highly attractive oxygenated monomers and obtain high-quality lignin under mild conditions. The study also showed that the selective modification of lignin enabled by plasma electrolysis could significantly improve the lignin valorization than the previous efforts for isolating the natural lignin. In future studies, techno-economic analysis and the process scalability will be further evaluated.

Conflicts of interest

There are no conflicts to declare.

Acknowledgements

The authors would like to acknowledge Dr. Sarah Cady from the Department of Chemistry at Iowa State University for NMR analyses, Dr. Haiyang Hu from the Department of Aerospace Engineering Department, and Daniel Vincent Sahayaraj from the Department of Chemical Engineering for technical discussions. The authors also acknowledge the instrument support from Bioeconomy Institute at Iowa State University. The research is partially supported by National Science Foundation grants 1803823 and 1826978.

References

- 1 R. C. Brown and T. R. Brown, *Biorenewable Resources*, John Wiley & Sons, Inc., Hoboken, NJ, USA, 2014, vol. 9781118524.
- 2 J. S. Luterbacher, D. Martin Alonso and J. A. Dumesic, *Green Chem.*, 2014, **16**, 4816–4838.
- 3 N. Srivastava, R. Rawat, H. Singh Oberoi and P. W. Ramteke, *Int. J. Green Energy*, 2015, **12**, 949–960.

- 4 E. Adler, *Wood Sci. Technol.*, 1977, **11**, 169–218.
- 5 P. Azadi, O. R. Inderwildi, R. Farnood and D. A. King, *Renewable Sustainable Energy Rev.*, 2013, **21**, 506–523.
- 6 A. V. Bridgwater, *Biomass Bioenergy*, 2012, **38**, 68–94.
- 7 R. Brown, *Thermochemical processing of biomass: conversion into fuels, chemicals and power*, John Wiley and Sons Inc., 2019.
- 8 A. Bridgwater, *Chem. Eng. J.*, 2003, **91**, 87–102.
- 9 A. N. Amenaghawon, C. L. Anyalewechi, C. O. Okieimen and H. S. Kusuma, *Environ. Dev. Sustainable*, 2021, **23**, 14324–14378.
- 10 R. Singh, A. Shukla, S. Tiwari and M. Srivastava, *Renewable Sustainable Energy Rev.*, 2014, **32**, 713–728.
- 11 A. Johansson, O. Aaltonen and P. Ylinen, *Biomass*, 1987, **13**, 45–65.
- 12 H. T. Tan and K. T. Lee, *Chem. Eng. J.*, 2012, **183**, 448–458.
- 13 A. Binder, L. Pelloni and A. Fiechter, *Eur. J. Appl. Microbiol. Biotechnol.*, 1980, **11**, 1–5.
- 14 A. Effendi, H. Gerhauser and A. V. Bridgwater, *Renewable Sustainable Energy Rev.*, 2008, **12**, 2092–2116.
- 15 G. W. Huber, S. Iborra and A. Corma, *Chem. Rev.*, 2006, **106**, 4044–4098.
- 16 J. Zakzeski, P. C. A. Bruijninx, A. L. Jongerius and B. M. Weckhuysen, *Chem. Rev.*, 2010, **110**, 3552–3599.
- 17 S. Zhou, Y. Xue, A. Sharma and X. Bai, *ACS Sustainable Chem. Eng.*, 2016, **4**, 6608–6617.
- 18 M. M. Abu-Omar, K. Barta, G. T. Beckham, J. S. Luterbacher, J. Ralph, R. Rinaldi, Y. Román-Leshkov, J. S. M. Samec, B. F. Sels and F. Wang, *Energy Environ. Sci.*, 2021, **14**, 262–292.
- 19 T. Renders, S. Van den Bosch, S.-F. Koelewijn, W. Schutyser and B. F. Sels, *Energy Environ. Sci.*, 2017, **10**, 1551–1557.
- 20 T. Renders, G. Van den Bossche, T. Vangeel, K. Van Aelst and B. Sels, *Curr. Opin. Biotechnol.*, 2019, **56**, 193–201.
- 21 Y. Huang, Y. Duan, S. Qiu, M. Wang, C. Ju, H. Cao, Y. Fang and T. Tan, *Sustainable Energy Fuels*, 2018, **2**, 637–647.
- 22 Y. Liu, G. Luo, H. H. Ngo, W. Guo and S. Zhang, *Bioresour. Technol.*, 2020, **298**, 122511.
- 23 J. D'Souza, R. Camargo and N. Yan, *Polym. Rev.*, 2017, **57**, 668–694.
- 24 A. C. Garcia, S. Cheng and J. S. Cross, *Clean Technol.*, 2020, **2**, 513–528.
- 25 T. Kan, V. Strezov and T. J. Evans, *Renewable Sustainable Energy Rev.*, 2016, **57**, 1126–1140.
- 26 C. M. Cai, T. Zhang, R. Kumar and C. E. Wyman, *Green Chem.*, 2013, **15**, 3140.
- 27 J. S. Luterbacher, J. M. Rand, D. M. Alonso, J. Han, J. T. Youngquist, C. T. Maravelias, B. F. Pfleger and J. A. Dumesic, *Science*, 2014, **343**, 277–280.
- 28 J. S. Luterbacher, A. Azarpira, A. H. Motagamwala, F. Lu, J. Ralph and J. A. Dumesic, *Energy Environ. Sci.*, 2015, **8**, 2657.
- 29 X. Bai, R. C. Brown, J. Fu, B. H. Shanks and M. Kieffer, *Energy Fuels*, 2014, **28**, 1111–1120.
- 30 Z. Chen, X. Bai, A. Lusi, W. A. Jacoby and C. Wan, *Bioresour. Technol.*, 2019, **289**, 121708.
- 31 F. Jérôme, *Curr. Opin. Green Sustainable Chem.*, 2016, **2**, 10–14.
- 32 J. Vanneste, T. Ennaert, A. Vanhulsel and B. Sels, *ChemSusChem*, 2017, **10**, 14–31.
- 33 K. Weltmann, J. F. Kolb, M. Holub, D. Uhrlandt, M. Šimek, K. (Ken) Ostrikov, S. Hamaguchi, U. Cvelbar, M. Černák, B. Locke, A. Fridman, P. Favia and K. Becker, *Plasma Processes Polym.*, 2019, **16**, 1800118.
- 34 I. Langmuir, *Proc. Natl. Acad. Sci. U. S. A.*, 1928, **14**, 627–637.
- 35 J. Meichsner, M. Schmidt, R. Schneider and H. E. Wagner, *Nonthermal Plasma Chemistry and Physics*, CRC Press, 2012.
- 36 A. Bogaerts, E. Neyts, R. Gijbels and J. van der Mullen, *Spectrochim. Acta, Part B*, 2002, **57**, 609–658.
- 37 R. Morent, N. De Geyter, T. Desmet, P. Dubruel and C. Leys, *Plasma Processes Polym.*, 2011, **8**, 171–190.
- 38 S. K. Pankaj, C. Bueno-Ferrer, N. N. Misra, V. Milosavljević, C. P. O'Donnell, P. Bourke, K. M. Keener and P. J. Cullen, *Trends Food Sci. Technol.*, 2014, **35**, 5–17.
- 39 B. Jiang, J. Zheng, S. Qiu, M. Wu, Q. Zhang, Z. Yan and Q. Xue, *Chem. Eng. J.*, 2014, **236**, 348–368.
- 40 T. von Woedtke, A. Schmidt, S. Bekeschus, K. Wende and K.-D. Weltmann, *In Vivo*, 2019, **33**, 1011–1026.
- 41 Y. Fan, W. Zhao, S. Shao, Y. Cai, Y. Chen and L. Jin, *Energy*, 2018, **142**, 462–472.
- 42 Y. Fan, Y. Xiong, L. Zhu, L. Fan, L. Jin, Y. Chen and W. Zhao, *Chem. Eng. Process.*, 2019, **135**, 53–62.
- 43 H. Taghvaei, M. Kheirollahivash, M. Ghasemi, P. Rostami and M. R. Rahimpour, *Energy Fuels*, 2014, **28**, 2535–2543.
- 44 X. Liu, T. He, Y. Ge, G. Li, J. Wu, Z. Wang, G. Liu and J. Wu, *J. Anal. Appl. Pyrolysis*, 2018, **131**, 128–133.
- 45 K. H. Becker, U. Kogelschatz, K. H. Schoenbach, R. J. Barker, U. Kogelschatz, K. H. Schoenbach and R. J. Barker, *Non-Equilibrium Air Plasmas at Atmospheric Pressure*, CRC Press, 2004.
- 46 K. Kolářová, V. Vosmanská, S. Rimpelová and V. Švorčík, *Cellulose*, 2013, **20**, 953–961.
- 47 M. Benoit, A. Rodrigues, Q. Zhang, E. Fourré, K. De Oliveira Vigier, J.-M. M. Tatibouët and F. Jérôme, *Angew. Chem., Int. Ed.*, 2011, **50**, 8964–8967.
- 48 W. W. Jun, Z. Fengcai and C. Bingqiang, *Plasma Sci. Technol.*, 2008, **10**, 743–747.
- 49 L. A. H. Hu and X. Bai, *Green Chem.*, 2020, **22**, 2036–2048.
- 50 I. Prasertsung, K. Aroonraj, K. Kamwilaisak, N. Saito and S. Damrongsakkul, *Carbohydr. Polym.*, 2019, **205**, 472–479.
- 51 I. Prasertsung, P. Chutinate, A. Watthanaphanit, N. Saito and S. Damrongsakkul, *Carbohydr. Polym.*, 2017, **172**, 230–236.
- 52 O. Takai, *Pure Appl. Chem.*, 2008, **80**, 2003–2011.
- 53 O. Takai, *J. Photopolym. Sci. Technol.*, 2014, **27**, 379–384.
- 54 D. Tang, X. Zhang and S. Yang, *Plasma Sci. Technol.*, 2018, **20**, 044002.
- 55 D. Xi, C. Jiang, R. Zhou, Z. Fang, X. Zhang, Y. Liu, B. Luan, Z. Feng, G. Chen, Z. Chen, Q. Liu and S. Yang, *Bioresour. Technol.*, 2018, **268**, 531–538.

- 56 D. Xi, R. Zhou, R. Zhou, X. Zhang, L. Ye, J. Li, C. Jiang, Q. Chen, G. Sun, Q. Liu and S. Yang, *Bioresour. Technol.*, 2017, **241**, 545–551.
- 57 L. A. H. Radhakrishnan, H. Hu, H. Hu and X. Bai, *Green Chem.*, 2020, **22**, 7871–7883.
- 58 A. Ghosh, X. Bai and R. C. Brown, *ChemistrySelect*, 2018, **3**, 4777–4785.
- 59 A. Ghosh, R. C. Brown and X. Bai, *Green Chem.*, 2016, **18**, 1023–1031.
- 60 H. Yui, Y. Someya, Y. Kusama, K. Kanno and M. Banno, *J. Appl. Phys.*, 2018, **124**, 103301.
- 61 P. Bruggeman, D. Schram, M. Á. González, R. Rego, M. G. Kong and C. Leys, *Plasma Sources Sci. Technol.*, 2009, **18**, 025017.
- 62 P. Bruggeman and C. Leys, *J. Phys. D: Appl. Phys.*, 2009, **42**, 053001.
- 63 M. Koch, M. Fischer and S. Tenbohlen, in *International Conference APTADM*, 2007.
- 64 F. Cao, T. J. Schwartz, D. J. McClelland, S. H. Krishna, J. A. Dumesic and G. W. Huber, *Energy Environ. Sci.*, 2015, **8**, 1808–1815.
- 65 M. A. Mellmer, C. Sener, J. M. R. Gallo, J. S. Luterbacher, D. M. Alonso and J. A. Dumesic, *Angew. Chem., Int. Ed.*, 2014, **53**, 11872–11875.
- 66 A. S. Mamman, J.-M. Lee, Y.-C. Kim, I. T. Hwang, N.-J. Park, Y. K. Hwang, J.-S. Chang and J.-S. Hwang, *Biofuels, Bioprod. Biorefin.*, 2008, **2**, 438–454.
- 67 J.-P. Lange, E. van der Heide, J. van Buijtenen and R. Price, *ChemSusChem*, 2012, **5**, 150–166.
- 68 M. B. Comba, Y. Tsai, A. M. Sarotti, M. I. Mangione, A. G. Suárez and R. A. Spanevello, *Eur. J. Org. Chem.*, 2018, **2018**, 590–604.
- 69 G. Dobeles, G. Rossinskaja, G. Telysheva, D. Meier, S. Radtke and O. Faix, in *Progress in Thermochemical Biomass Conversion*, Blackwell Science Ltd, Oxford, UK, 2008, pp. 1500–1508.
- 70 S. Kang, J. Fu and G. Zhang, *Renewable Sustainable Energy Rev.*, 2018, **94**, 340–362.
- 71 M. J. Taherzadeh and K. Karimi, *Bioresour. Technol.*, 2007, **2**, 472–499.
- 72 A. Ozkan, T. Dufour, T. Silva, N. Britun, R. Snyders, A. Bogaerts and F. Reniers, *Plasma Sources Sci. Technol.*, 2016, **25**, 025013.
- 73 B. Hu, Q. Lu, Y. Wu, W. Xie, M. Cui, J. Liu, C. Dong and Y. Yang, *J. Energy Chem.*, 2020, **43**, 78–89.
- 74 J. He, M. Liu, K. Huang, T. W. Walker, C. T. Maravelias, J. A. Dumesic and G. W. Huber, *Green Chem.*, 2017, **19**, 3642–3653.
- 75 W. Ying, *Funct. Mater.*, 2016, **23**, 344–349.
- 76 H. B. Mayes and L. J. Broadbelt, *J. Phys. Chem. A*, 2012, **116**, 7098–7106.
- 77 J. Rencoret, G. Marques, A. Gutiérrez, L. Nieto, J. Jiménez-Barbero, Á. T. Martínez and J. C. del Río, *Ind. Crops Prod.*, 2009, **30**, 137–143.
- 78 A. Fujimoto, Y. Matsumoto, H.-M. Chang and G. Meshitsuka, *J. Wood Sci.*, 2005, **51**, 89–91.
- 79 X. Bai, K. H. Kim, R. C. Brown, E. Dalluge, C. Hutchinson, Y. J. Lee and D. Dalluge, *Fuel*, 2014, **128**, 170–179.
- 80 L. Shuai and B. Saha, *Green Chem.*, 2017, **19**, 3752–3758.
- 81 K. H. Kim, X. Bai and R. C. Brown, *J. Anal. Appl. Pyrolysis*, 2014, **110**, 254–263.
- 82 H. Kawamoto, *J. Wood Sci.*, 2017, **63**, 117–132.
- 83 T. Kotake, H. Kawamoto and S. Saka, *J. Anal. Appl. Pyrolysis*, 2013, **104**, 573–584.
- 84 L. Shuai, M. T. Amiri, Y. M. Questell-Santiago, F. Héroguel, Y. Li, H. Kim, R. Meilan, C. Chapple, J. Ralph and J. S. Luterbacher, *Science*, 2016, **354**, 329–333.
- 85 A. Beste and A. C. Buchanan, *J. Org. Chem.*, 2009, **74**, 2837–2841.
- 86 S. Wang, K. Zhang, H. Li, L.-P. Xiao and G. Song, *Nat. Commun.*, 2021, **12**, 416.
- 87 C. Cheng, J. Wang, D. Shen, J. Xue, S. Guan, S. Gu and K. H. Luo, *Polymers*, 2017, **9**, 38–50.
- 88 R. Ma, M. Guo and X. Zhang, *Catal. Today*, 2018, **302**, 50–60.
- 89 Q. Xiang and Y. Y. Lee, *Appl. Biochem. Biotechnol.*, 2000, **84–86**, 153–162.
- 90 P. J. Deuss and K. Barta, *Coord. Chem. Rev.*, 2016, **306**, 510–532.
- 91 C. Xu, R. A. D. Arancon, J. Labidi and R. Luque, *Chem. Soc. Rev.*, 2014, **43**, 7485–7500.
- 92 V. M. Roberts, V. Stein, T. Reiner, A. Lemonidou, X. Li and J. A. Lercher, *Chem. – Eur. J.*, 2011, **17**, 5939–5948.
- 93 D. M. Alonso, S. G. Wettstein and J. A. Dumesic, *Green Chem.*, 2013, **15**, 584.
- 94 C. Li, X. Zhao, A. Wang, G. W. Huber and T. Zhang, *Chem. Rev.*, 2015, **115**, 11559–11624.
- 95 Y. Jing, L. Dong, Y. Guo, X. Liu and Y. Wang, *ChemSusChem*, 2020, **13**, 4181–4198.